Appl. Math. Mech. -Engl. Ed., **41**(9), 1287–1302 (2020)

APPLIED MATHEMATICS AND MECHANICS (ENGLISH EDITION)

https://doi.org/10.1007/s10483-020-2644-8

Improving control effects of absence seizures using single-pulse alternately resetting stimulation (SARS) of corticothalamic circuit*

Denggui FAN[1], Yanhong ZHENG[2], Zecheng YANG[1], Qingyun WANG[3,†]

1. School of Mathematics and Physics, University of Science and Technology Beijing, Beijing 100083, China;
2. College of Mathematics and Informatics, Fujian Normal University, Fuzhou 350117, China;
3. Department of Dynamics and Control, Beihang University, Beijing 100191, China

(Received Mar. 13, 2020 / Revised May 28, 2020)

Abstract Presently, we develop a simplified corticothalamic (SCT) model and propose a single-pulse alternately resetting stimulation (SARS) with sequentially applying anodic (A, "+") or cathodic (C, "−") phase pulses to the thalamic reticular (RE) nuclei, thalamus-cortex (TC) relay nuclei, and cortical excitatory (EX) neurons, respectively. Abatement effects of ACC-SARS of RE, TC, and EX for the 2 Hz–4 Hz spike and wave discharges (SWD) of absence seizures are then concerned. The m:n on-off ACC-SARS protocol is shown to effectively reduce the SWD with the least current consumption. In particular, when its frequency is out of the 2 Hz–4 Hz SWD dominant rhythm, the desired seizure abatements can be obtained, which can be further improved by our proposed directional steering (DS) stimulation. The dynamical explanations for the SARS induced seizure abatements are lastly given by calculating the averaged mean firing rate (AMFR) of neurons and triggering averaged mean firing rates (TAMFRs) of 2 Hz–4 Hz SWD.

Key words epileptic absence seizure, spike and wave discharge (SWD), single-pulse alternately resetting stimulation (SARS), mean field model, averaged mean firing rate (AMFR), seizure control

Chinese Library Classification O175, O322
2010 Mathematics Subject Classification 37H20, 37N25, 34D10, 34D20

1 Introduction

Absence seizures are characterized by about 2 Hz–4 Hz spike and wave discharges (SWD)[1–2] which are correlated with the pathologic oscillations within the corticothalamic (CT) circuit[3–5]. It is prevailing that most neurological disorders are associated with altered brain dynamics[6–8].

* Citation: FAN, D. G., ZHENG, Y. H., YANG, Z. C., and WANG, Q. Y. Improving control effects of absence seizures using single-pulse alternately resetting stimulation (SARS) of corticothalamic circuit. *Applied Mathematics and Mechanics* (*English Edition*), **41**(9), 1287–1302 (2020) https://doi.org/10.1007/s10483-020-2644-8

† Corresponding author, E-mail: nmqingyun@163.com

Project supported by the National Natural Science Foundation of China (Nos. 11702018, 11932003, and 11672074)

Intensive investigations with the control mechanism underlying the neuronal interactions by deep brain stimulation (DBS) have been performed[9–11], which revealed that the DBS could restore the aberrant activity in brain. In particular, it is shown to suppress the epileptic seizures by modulating the targeted structures[12–16]. However, the dynamic mechanism underlying the DBS modulation is still enigmatic. As such, how to identify the appropriate stimulation targets is still a pending issue. Although the DBS has been empirically applied to thalamus[14–15] and neocortex[16], the combined effect of both cortex and thalamus stimulations on seizures has rarely been reported. Also, the functions of autaptic connections of cortex or thalamus on seizures are unknown even though seizures are believed to be caused by the reverberatory activity of thalamus-cortex (TC) loop.

In addition, Chen et al.[17–18] developed a basal ganglia-corticothalamic (BG-CT) mean field model. The schematic of BG-CT circuit is shown in Fig. 1(a), where CT not only includes cortical excitatory (EX) and inhibitory (IN) neurons, but also is comprised of the TC relay nuclei and thalamic reticular (RE) neurons. It was computationally revealed that BG played the modulating action for the CT circuit entraining absence seizures. In particular, as shown in Fig. 1(a) (also see Fig. 1 in Ref. [18]), after receiving 2 glutamatergic projections from CT, basal ganglia (BG) sends 3 gamma-aminobutyric acidergic (GABAergic) projections back to it. This suggests that the 3 GABAergic modulations from BG can be replaced by 3 adscititious stimulations. We hence develop a simplified corticothalamic (SCT) mean field model, which is obtained by replacing the input modulations from BG with anodic (A,"+") or cathodic (C, "−") phase single-pulse stimulation applied on RE, TC, and EX, respectively.

Based on this SCT model, the aforementioned questions are addressed by proposing a tri-target single-pulse alternately resetting stimulation (SARS) strategy. Then, we comprehensively investigate the combined effects of autaptic connections of cortex and thalamus on SWD generations as well as the SWD abatement by using the SARS on them. Our work is also motivated by a desire to optimize the spatiotemporal pattern of the SARS with the aim of improving its control effect for the SWD, and finally to reveal the dynamic mechanisms underlying seizure control.

2 Model and method

2.1 Mean field model

The mean field approach is used to model the absence seizures, because the generalized seizure is the dynamic expression of hyper-consistent activity of a huge number of neurons. As shown in Fig. 1(a), the SCT mean field model can describe the dynamics of thalamic and cortical neural masses. The thalamus consists of both glutamatergic TC and GABAergic RE masses. The cortex includes both EX and IN masses. In the current study, the brain activity of generalized absence seizures is determined by spatially uniform activity over several selective cortical networks[19]. Therefore, the dynamical variables of neural masses are supposed to depend only on time. In particular, these neural masses are simulated by the mean membrane potential $V(t)$ which further determines the mean firing rate (MFR) $R(t)$ and the axonal field $\phi(t)$. Hence, the SCT system is governed by the following four second-order differential equations with the time delay:

$$\begin{cases} \phi_{\rm e}''(t) = -2\gamma_{\rm e}\phi_{\rm e}'(t) - \gamma_{\rm e}^2\phi_{\rm e}(t) + \gamma_{\rm e}^2\Gamma(V_{\rm e}(t)), \\ V_{\rm e}''(t) = \alpha\beta(\nu_{\rm ee}\phi_{\rm e} + \nu_{\rm ei}\Gamma(V_{\rm i}) + \nu_{\rm et}\Gamma(V_{\rm t}) - V_{\rm e}(t) + S_{\rm e}(t)) - (\alpha+\beta)V_{\rm e}'(t), \\ V_{\rm t}''(t) = \alpha\beta(\nu_{\rm te}\phi_{\rm e} + \nu_{\rm tr}^{\rm A}\Gamma(V_{\rm r}) + \nu_{\rm tr}^{\rm B}\Gamma(V_{\rm r}(t-\tau)) - V_{\rm t}(t) + P_{\rm n} + S_{\rm t}(t)) - (\alpha+\beta)V_{\rm t}'(t), \\ V_{\rm r}''(t) = \alpha\beta(\nu_{\rm re}\phi_{\rm e} + \nu_{\rm rt}\Gamma(V_{\rm t}) - V_{\rm r}(t) + S_{\rm r}(t)) - (\alpha+\beta)V_{\rm r}'(t). \end{cases} \tag{1}$$

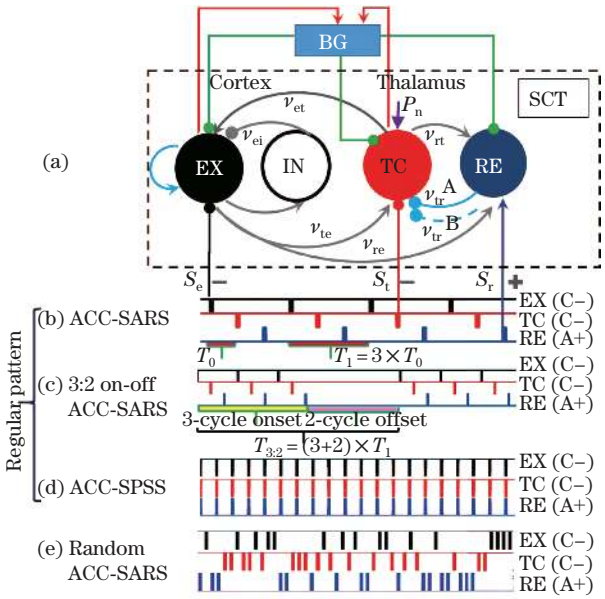

Fig. 1 Schematics of BG-CT circuits and SCT models: (a) arrows represent glutamatergic projection actions. Lines with circles depict GABAergic projection actions, where solid and dashed ones correspond to mediations of $GABA_A$ and $GABA_B$, respectively. Synaptic strengths between different populations are denoted by ν_{ee}, ν_{tr}, etc. S_e, S_t, and S_r represent the adscititious neurostimulations. $P_n = 2$ mV·s denotes the nonspecific subthalamic input to TC; (b) regular ACC-SARS (ACC represents anodic (A, "+", blue)-cathodic (C, "−", red)-cathodic (C, "−", black)); (c) 3∶2 on-off ACC-SARS; (d) ACC-SPSS (SPSS represents the single-pulse parallelly and simultaneously stimulation) with the electrodes being parallelly and simultaneously activated; (e) random ACC-SARS with the electrodes being randomly and alternately activated (color online)

The MFR $R_x(t)$ of these neural masses is estimated by their $V_x(t)$ as

$$R_x(t) = \Gamma(V_x(t)) = \frac{R_x^{\max}}{1 + \exp\left(-\dfrac{\pi(V_x(t) - \Theta_x)}{\sqrt{3}\sigma_x}\right)}, \tag{2}$$

where $x =$ e, i, t, and r, Θ_x and σ_x describe the MFR thresholds, and $R_x^{\max}$ represents the maximum of firing rate of neural mass. In turn, V_x is influenced by both the incoming pulse from the related other neural masses and the electrical pulse inputs $S_x(t)$. Thus, it can be determined by

$$\mathrm{D}_{\alpha\beta} V_x(t) = \sum_{y=\mathrm{e,i,t,r}} \nu_{xy}\phi_y(t) + S_x(t), \tag{3}$$

where the operator

$$\mathrm{D}_{\alpha\beta} = \frac{1}{\alpha\beta}\left(\frac{\mathrm{d}^2}{\mathrm{d}t^2} + (\alpha+\beta)\frac{\mathrm{d}}{\mathrm{d}t} + \alpha\beta\right) \tag{4}$$

reflects the filtering effect of incoming pulses through dendrite, α and β are the corresponding response times, $\phi_y(t)$ is the incoming pulse rate generated by the neural mass y, and acted on the other neural mass x, and ν_{xy} describes the synaptic strength of incoming pulses from y acted on x. In addition, similar to the previous works[20–22], the SCT model is reduced by

assuming $V_{\rm i} = V_{\rm e}$ and $R_{\rm i} = R_{\rm e}$ due to the proportional relationship between their involved synapses, which allows us to neglect $V_{\rm i}$.

IN, TC, and RE have too short axons, thus,

$$\phi_z(t) \approx R_z(t) = \Gamma(V_z(t)), \tag{5}$$

where $z =$ i, t, and r. However, $\phi_{\rm e}$ is governed by

$$\frac{1}{\gamma_{\rm e}^2}\Big(\frac{{\rm d}^2}{{\rm d}t^2} + 2\gamma_{\rm e}\frac{\rm d}{{\rm d}t} + \gamma_{\rm e}^2\Big)\phi_{\rm e}(t) = R_{\rm e}(t) = \Gamma(V_{\rm e}(t)) \tag{6}$$

due to the non-ignorable propagation effect when $R_{\rm e}$ propagates on the mean axonal length of $l_{\rm e}$ at the velocity of $v_{\rm e}$. Here, $\gamma_{\rm e} = v_{\rm e}/l_{\rm e}$. Therefore, we have four effective variables, i.e., $V_{\rm e}$, $V_{\rm t}$, $V_{\rm r}$, and $\phi_{\rm e}$. The incoming pulse rates from RE to TC are denoted by $\phi_{\rm r}(t)$ and $\phi_{\rm r}(t-\tau)$, where τ is due to the delayed mediation of $\rm GABA_B$ via the second messenger processes compared with $\rm GABA_A$. However, both the numbers of projections are supposed to be the same, i.e., $\nu_{\rm tr}^{\rm A} = \nu_{\rm tr}^{\rm B}$, denoted as $\nu_{\rm tr}$.

2.2 SARS stimulation setup

As shown in Fig. 1, for instance, the SCT model is obtained by replacing the input modulations from BG with ACC-SARS applied on RE, TC, and EX, respectively, i.e., r+, t−, and e−. In particular, as seen from Fig. 1(b), the regular SARS pulses applied to RE, TC, and EX of the SCT model are described by $S_{\rm r}(t)$, $S_{\rm t}(t)$, and $S_{\rm e}(t)$, respectively. The SARS protocol is modeled as

$$S_{\rm SARS}(t) = \sum_{x={\rm r,t,e}} \xi_x(t) S_x(t). \tag{7}$$

Here, we term $\xi_x(t)$ as the indicator, where $\xi_x(t) = 1$, if electrode (contact) x is active at time t, or $\xi_x(t) = 0$. In one period of SARS, 3 electrodes or 3 contacts in one electrode applied to RE, TC, and EX, respectively, are alternately and sequentially activated, and only one pulse is received by each nucleus. Then, we can build a periodic SARS stimulation pattern by repeating this procedure. $S_x(t)$ is the rectangular pulse train[23–24],

$$S_x(t) = S_0(H(\sin(2\pi t/T_0)) \times (1 - H(\sin(2\pi(t+\delta_0)/T_0)))), \tag{8}$$

where T_0 and δ_0 denote the pulse period and the duration, respectively. $S_0 > 0$ or $S_0 < 0$ represents the pulse strength of anodic or cathodic phases. H is a step function, where if $x > 0$, $H(x) = 1$, otherwise $H(x) = 0$. Note that, in one period of regular SARS, the switching duration of alternate activations of electrode among 3 neural masses is equal to the pulse period of $S_x(t)$, i.e., T_0. Thus, the period of SARS is $T_1 = 3T_0$. In particular, if we perform m cycles of periodic regular SARS (with the stimulation on) followed by n cycles (with the stimulation off), we can obtain the novel stimulation pattern termed as $m\!:\!n$ on-off SARS (e.g., $m\!:\!n$=3:2 in Fig. 1(c)). Its period is calculated as $(m+n) \times T_1$. By contrast, if the electrodes applied to RE, TC, and EX are randomly activated, the random SARS is modeled (see Fig. 1(e)), where each nucleus may receive one to three pulses continuously in the same one period of regular SARS. In addition, if the 3 electrodes are parallelly and simultaneously activated, the SPSS (see Fig. 1(d)) pattern is modeled, where in the same one period of regular SARS, each nucleus can receive three pulses continuously. Unless otherwise specified, all SARS, $m\!:\!n$ on-off SARS, and SPSS refer to the regular stimulation patterns. Numerically, $m\!:\!n$ on-off SARS can be simulated by[25]

$$S_{\rm SARS}(m,n,t) = S_x(t){\rm sgn}(\prod_{k=0}^{n-1}((m+n)-k-y)). \tag{9}$$

Here, $x = I_{\rm nt}((t - I_{\rm nt}(t/T_1)\cdot T_1)/T_0) + 1$, and $y = I_{\rm nt}((t - I_{\rm nt}(t/T_{m:n})\cdot T_{m:n})/T_1) + 1$, where $I_{\rm nt}$ is a round function, $T_{m:n}$ is the period of $m\!:\!n$ on-off SARS calculated by $T_1 \cdot (m+n)$, and sgn satisfies ${\rm sgn}(\mathbf{N}^+) = 1$ and ${\rm sgn}(\mathbf{R} \setminus \mathbf{N}^+) = 0$.

2.3 SWD control and current consumption indexes

To facilitate observation for SWD abatement using stimulations, we mesh the parametric plane into well-proportioned grid points. Thus, the grid points of the model displaying the SWD can be counted. In particular, we use the following SWD control percentage to quantitatively assess the SWD abatement effects of stimulus[26]:

$$\eta = (1 - W/U) \times 100\%, \tag{10}$$

where U and W represent the grid points of the model displaying the SWD in the absence and presence of stimulus, respectively. $\eta > 0$ means the success of SWD control while $\eta < 0$ suggests that stimulus can promote seizures. In addition, to give a comprehensive control evaluation for the proposed stimulation protocols, we also consider the current consumption computed as follows:

$$Q(t) = \int_0^{t_{\rm end}} \sum_{x={\rm e,t,r}} |S_x(t)| {\rm d}t \tag{11}$$

with the unit of V·s. In this paper, $t_{\rm end} = 25$ s is the stimulation duration.

2.4 Simulation method

A simulation time duration of 25 s with the step of 0.05 ms is performed using the four-stage Runge-Kutta iterative method. Model parameters are listed in Table 1. The 2 Hz–4 Hz SWD solution is particularly concerned due to the resembling electroencephalogram (EEG) activity of brain seizures. Since we wish to reveal the critical transitions between the 2 Hz–4 Hz SWD and the other states, state bifurcation is calculated using the stable state beginning at $t = 5$ s with respect to the key parameters. In particular, the bifurcation diagram is charted by searching for the local extrema of $\phi_{\rm e}$. We also investigate the dynamical features corresponding to different states using AUTO in XPPAUT (a software package[27]). Furthermore, we also give the dominant frequency of neural masses, which is calculated by the fast Fourier transform (FFT) of $\phi_{\rm e}(t)$.

Table 1 Interpretations and standard values of parameters

Parameter	Interpretation	Standard value
$R_x^{\max}$/Hz, x =e, i, t, r	MFR	250
Θ_x, σ_x/mV	Threshold variables of MFR	Θ_x=15, σ_x=6
$\alpha, \beta/{\rm s}^{-1}$	Response times of incoming pulses	α=50, β=200
$\gamma_{\rm e}$/Hz	Cortical pulses' attenuation rate	100
τ/ms	Time delay mediated by $GABA_B$ synapses	50
$P_{\rm n}/({\rm mV\cdot s})$	Nonspecific subthalamic input onto TC	2
$\nu_{\rm ee}/({\rm mV\cdot s})$	EX → EX coupling strength	0.5–1
$-\nu_{\rm tr}/({\rm mV\cdot s})$	RE → TC coupling strength	0.3–1.2
$-\nu_{\rm ei}/({\rm mV\cdot s})$	IN → EX coupling strength	1.8
$\nu_{\rm re}/({\rm mV\cdot s})$	EX → RE coupling strength	0.05
$\nu_{\rm rt}/({\rm mV\cdot s})$	TC → RE coupling strength	0.5
$\nu_{\rm te}/({\rm mV\cdot s})$	EX → TC coupling strength	2.2
$\nu_{\rm et}/({\rm mV\cdot s})$	TC → EX coupling strength	1.8

Another wish is to employ stimulation to control the 2 Hz–4 Hz SWD onset. We can notice that the different firing states correspond to their deterministic evolutions of typical MFRs, i.e., axonal field ϕ. The 2 Hz–4 Hz dominant frequency is in fact the evolution frequency of TC MFR of SWD over time. Here, we will calculate the averaged mean firing rate (AMFR) corresponding to the 2 Hz–4 Hz SWD for each neural mass from 5 s to 25 s. By appropriately

intervening AMFRs, the rhythmic SWD may be calmed. In particular, the AMFR of neural masses may be increased or decreased with the increasing bifurcation parameter. Hence, the low and high triggering averaged mean firing rates (TAMFRs) of 2 Hz–4 Hz SWD for each neural mass can be determined by the critical AMFRs occurring at the boundaries of the SWD state bifurcation.

3 Results

3.1 Bifurcations related to SWD induced by both autaptic connections of thalamus and neocortical pyramidal neurons

We start by examining how the connectivity dynamics of CT circuit can induce the SWD of absence seizures. Firstly, the $\mathrm{GABA_{A/B}}$ effect acted on TC from RE (autaptic connection of thalamus), $-\nu_{\mathrm{tr}}$, has been demonstrated to incur the brain activity of the typical 2 Hz–4 Hz SWD[28–29] due to the double but independent $\mathrm{GABA_A}$- and $\mathrm{GABA_B}$-mediated functions with a significant delay, $\tau = 50$ ms. We therefore make the bifurcation analysis with respect to $-\nu_{\mathrm{tr}}$, as depicted in Figs. 2(a) and 2(b). When $-\nu_{\mathrm{tr}}$ is too small, the RE inhibition cannot

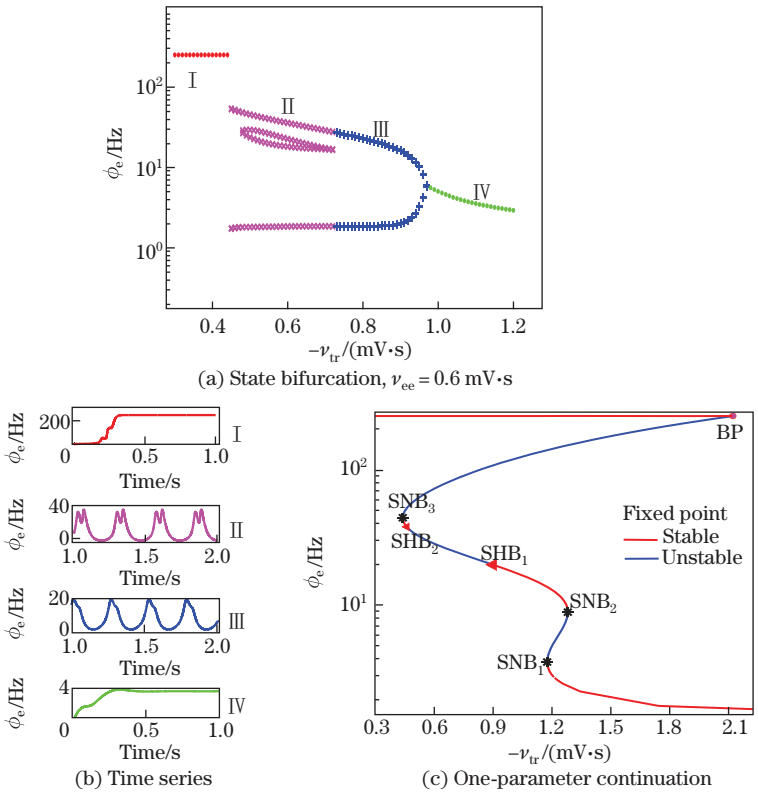

Fig. 2 (a) Bifurcation chart of ϕ_{e} with respect to the GABAergic projection strength of RE-TC, $-\nu_{\mathrm{tr}}$, with fixing $\nu_{\mathrm{ee}} = 0.6$ mV·s. Insets show four dynamical states, i.e., (I) the saturation state, (II) the SWD, (III) the simple oscillation, and (IV) the low firing state; (b) $-\nu_{\mathrm{tr}} \in [0.3$ mV·s, 1.2 mV·s] corresponding to these four dynamical states can take, e.g., (I) $-\nu_{\mathrm{tr}} = 0.3$ mV·s, (II) $-\nu_{\mathrm{tr}} = 0.5$ mV·s, (III) $-\nu_{\mathrm{tr}} = 0.8$ mV·s, and (IV) $-\nu_{\mathrm{tr}} = 1.2$ mV·s. Unless otherwise stated, other parameter values are listed in Table 1; (c) dynamics bifurcation diagram of ϕ_{e} involving a series of saddle node bifurcations (SNBs) and subcritical Hopf bifurcations (SHBs) (color online)

effectively suppress the TC firing. Thus, the recurrent excitations between TC and EX can excite EX activity to the saturate level (see Region I). As $-\nu_{\rm tr}$ grows, $\rm GABA_A$ first affects TC, then the MFR of TC decreases a little. TC successively inhibits and decreases the MFR of EX, which, however, recovers soon under both the autaptic function of EX, $\nu_{\rm ee}$, and the recurrent excitation between TC and EX. This ultimately induces the spike component of SWD complex (see Region II). After $\tau = 50$ ms later, $\rm GABA_B$ joins into the GABAergic actions on TC, and their combined inhibitions can make the MFR of TC have a large and prolonged decrease. TC can further shape the firing of EX. Then, the autaptic function of EX and recurrent excitation between TC and EX can slowly restore the MFR of EX. Thus, the slow wave component of SWD complex is induced. Additionally, for large $-\nu_{\rm tr}$, the strong inhibition can prolong the intra-thalamus recurrent excitations recovery, which will induce the partial fusion of the $\rm GABA_A$ and $\rm GABA_B$ signals. Then, the system is deteriorated to the simple oscillations (see Region III). However, if $-\nu_{\rm tr}$ is too large, TC firing is largely inhibited. Then, the system is cooled to the low activity level (see Region IV). The dynamical bifurcation analysis confirms that the GABAergic projections from RE to TC change the intrinsic firing properties of the EX neural mass through a series of SHBs and SNBs (see Fig. 2(c)).

In addition, autapses of neocortical pyramidal neurons, e.g., $\nu_{\rm ee}$, have been shown by recent experimental findings[30–31] to be an important functional circuit element that can enhance burst firings. To check whether $\nu_{\rm ee}$ can also contribute to the generation of the SWD, the bi-parameter bifurcation on the plane of $(-\nu_{\rm tr}, \nu_{\rm ee})$ is performed (see Fig. 3(a)). The dominant frequency (see Fig. 3(b)) is also computed to differentiate the various states. It is seen from Fig. 3(a) that the above-identified four states correspond to the four regions of the panel of $(-\nu_{\rm tr}, \nu_{\rm ee})$. It is obvious that similar state transitions to Fig. 2(a) can be obtained for each fixed $\nu_{\rm ee}$. However, as $\nu_{\rm ee}$ grows, the parametric region corresponding to the 2 Hz–4 Hz SWD (see Region II) is gradually enlarged. As analyzed above, this is because the increasing autaptic excitation of EX can indirectly relieve the inhibitions of RE to TC, which separates the $\rm GABA_A$- and $\rm GABA_B$-mediated signals and induces the SWD. This demonstrates that autaptic excitation of EX of cortex can shape the firing of EX neural mass.

3.2 SWD control effect of ACC-SARS on RE, TC, and EX

3.2.1 Rationality for ACC-SARS setup

We then turn to evaluate the DBS abatement on the SWD. During simulations, the $(-\nu_{\rm tr}, \nu_{\rm ee})$ panel is finely meshed into 10×11 parametric points. Moreover, the number of SWD can be quantitatively counted as 40. To clearly observe the SWD abatement, as an example, we employ a rectangle pulse train with the cathodic phase to TC (see the middle panel of Fig. 1(d)) on the same $(-\nu_{\rm tr}, \nu_{\rm ee})$ panel. By comparing Fig. 3(c) with Fig. 3(a), it is seen that, under the condition of stimulation, the 2 Hz–4 Hz SWD region is greatly reduced (see Region $\rm II_1$ in Fig. 3(c)), and the number of SWD is decreased from 40 to 14. At the same time, pulse stimulation drives the simple oscillation (III in Fig. 3(a)) and 2 Hz–4 Hz SWD (II in Fig. 3(a)) into the low firing states (VI in Fig. 3(c)) and <2 Hz SWD ($\rm II_2$ in Fig. 3(c)), respectively. Figure 4(a) shows that, as the pulse frequency of TC cathodic - phase stimulation (t −) increases, the SWD can be gradually abated and completely controlled ($\eta = 100\%$, counted by Eq. (10)) as $f_{\rm r}^0 \geqslant 40$ Hz. Similar scenarios can be observed for the case of EX cathodic-phase stimulation (e−). Unsurprisingly, these two cases are consistent with the previous analysis for the BG modulation which projects GABAergic functions to TC and EX neural masses, respectively. In addition, even though BG also projects inhibitions to RE, Fig. 4(a) shows that RE anodic - phase stimulation (r+) is superior to cathodic-phase stimulation (r−) which can only partly control the SWD. Therefore, based on this finding, we propose a tri-target SARS with anodic(A)-phase, cathodic(C)-phase, and cathodic(C)-phase pulses applied to RE, TC, and EX, respectively, termed as ACC-SARS (see Fig. 1(b)). The combined effects of tri-target ACC-SARS stimulation are particularly concerned. As Fig. 4(a) shows that when $f^0 \geqslant 50$ Hz, all stimulations (r+, t−, and e−) can almost completely control the SWD, in what follows, the switching frequency of

SARS, i.e., T_0 in Eq. (8) is always set as $1/f^0 = 20$ ms. By the way, the concurrent stimulations of ACC-SPSS (see Fig. 1(d)) with f^0=50 Hz can also completely control the SWD.

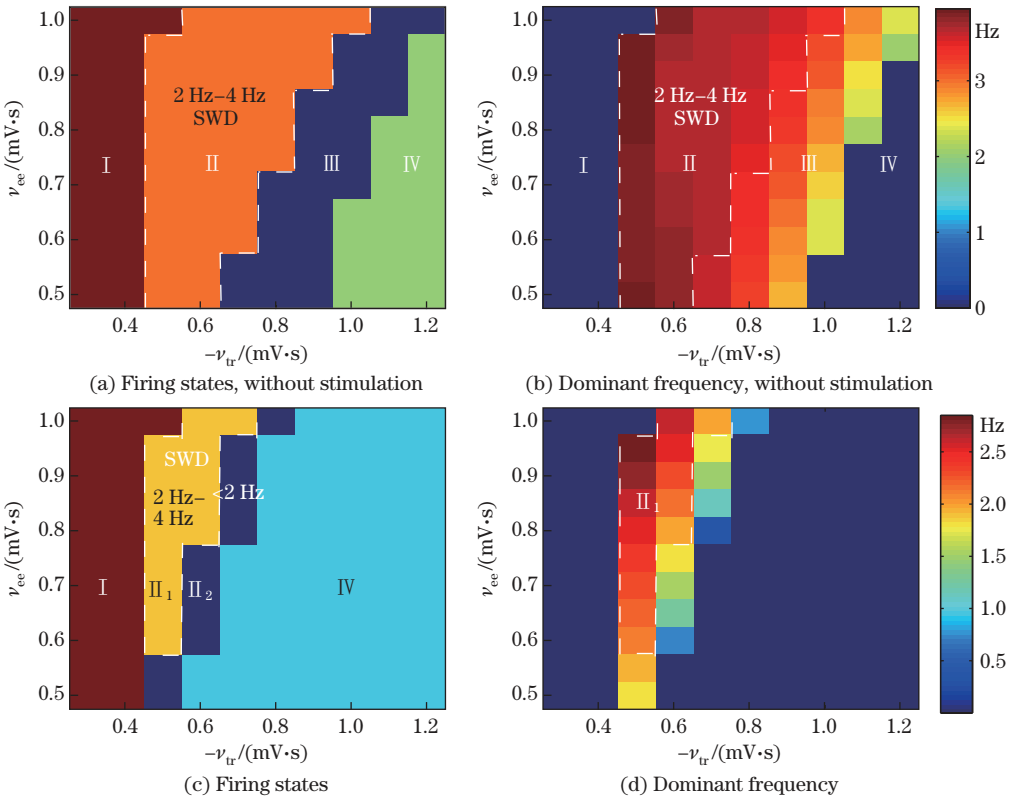

(a) Firing states, without stimulation (b) Dominant frequency, without stimulation

(c) Firing states (d) Dominant frequency

Fig. 3 (a) and (c) the state bifurcation and (b) and (d) frequency analysis of ϕ_e in the $(-\nu_{tr}, \nu_{ee}) \in [0.3\,\text{mV·s}, 1.2\,\text{mV·s}] \times [0.5\,\text{mV·s}, 1\,\text{mV·s}]$ panel, (a) and (b) without stimulation and (c) and (d) with a cathodic-phase single sequence pulse stimulation applied only on TC, i.e., t−, which can be simulated by setting $\delta_0 = 1$ ms, $S_0 = -150$ mV, and $f^0 = 30$ Hz in Eq. (8). (I) saturation state, (II_1) 2 Hz–4 Hz SWD, corresponding to the white line shaped regions, (II_2) <2 Hz SWD, (III) simple oscillation, and (IV) low firing state, where the numbers of SWD in Figs. 3(a) and 3(b) are 40, while the ones in Figs. 3(c) and 3(d) are 14 (color online)

3.2.2 SWD abatement effect of $m:n$ on-off ACC-SARS

However, compared with ACC-SPSS, if ACC-SARS has a comparable effect in controlling the SWD, it will cost much less current. Figure 4(b) gives the random ACC-SARS (see Fig. 1(e)), which, unfortunately, is shown to have almost no effect on SWD abatement. Naturally, we then turn to the regular ($m:n$ on-off) ACC-SARS (see Figs. 1(b) and 1(c)). Whereas, before that we first consider a general spatiotemporally patterned stimulation as shown in Fig. 5(a), which is not exactly the same to SARS and generated by setting $T_1 = 36$ ms in Eq. (9). It is surprisingly shown that this stimulation can completely control the SWD, even though it consumes as many currents as the random ACC-SARS. To further reduce the current consumption in the premise of maintaining the perfect control effect on the SWD, more sparse stimulation patterns by adjusting the ratio of $m:n$ $(m, n = 1, 2, \cdots, 5)$ in Eq. (9) are considered (e.g., the case of $m:n$=3:2 in Fig. 5(a)). Figure 5(b) shows that almost half the $m:n$ combinations can effectively control the SWD and a fifth of that can completely abate the SWD. In particular, from Fig. 5(c), we can see that the current consumed by the case of $m:n$=2:2 is half that of general case from the panel of Fig. 5(a). However, we also observe from Fig. 5(b) that in

some cases of $m{:}n$ combinations, the SWD number almost doubles (i.e., $\eta \approx -100\%$). To further improve the control effect, we enhance the pulse train parameters. Figures 5(d)–5(f) give the results corresponding to $T_1 = 60\,\text{ms}$ in Eq. (9) which generates the standard ($m{:}n$ on-off) ACC-SARS (see Fig. 5(d)). By contrast, Fig. 5(e) shows that, in this case, more $m{:}n$ combinations (3/5) can completely abate the SWD. This leads to the more broader flexibility of optimal parameter choice even though it may consume more currents as seen from Fig. 5(f). Furthermore, Figs. 5(g) and 5(h) give the relationship between the period of $m{:}n$ on-off ACC-SARS (i.e., $(m+n)\times T_1$) and the dominant rhythm of 2 Hz–4 Hz SWD in effectively controlling SWD onsets, which consistently shows that the frequency of $m{:}n$ on-off ACC-SARS out of the 2 Hz–4 Hz dominant rhythm interval is obviously the better choice.

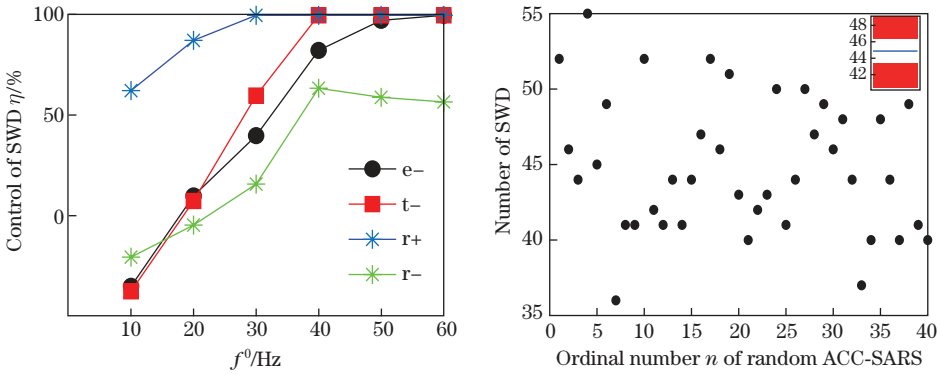

(a) Control of SWD (b) Random ACC-SARS

Fig. 4 (a) The control of SWD (calculated by Eq. (10)) under the condition of a single sequence pulse stimulation applied on RE, TC, and EX with scanning f^0 in [10 Hz, 100 Hz] and fixing $\delta_0 = 1\,\text{ms}$, as well as taking $S_0 = 150\,\text{mV}$ (r+) and $S_0 = -150\,\text{mV}$ (r−, t−, e−), respectively; (b) the SWD abatement of random ACC-SARS (see Fig. 1(e)) applied on RE, TC, and EX, i.e., r+, t−, e− with $\delta = 1\,\text{ms}$, $|S_0| = 150\,\text{mV}$, and $f^0 = 1/T_0 = 50\,\text{Hz}$. The number of SWD with no stimulus is 40 (control). 40 independent simulations are carried out to obtain the convincing results, i.e., the scattered black dots. Error bar (inset) shows that the average is 45 (color online)

3.2.3 Improved effects of directional steering (DS) SARS

Note that, the pulse intensity and width in each $m{:}n$ on-off ACC-SARS are relatively invariable. Figure 6(a) shows the SWD attractor on the phase space spanned by RE, TC, and EX. The abatement of SWD is correlated with the change of its shape. Here, SWD oscillation is of the typical spike and wave complex. Hence, to abate the SWD is in fact to make the system transit into the background resting state or other rhythmic activities which all involve in the change of the SWD shape. Thereby, the needed stimulus strengths pointed to RE, TC, and EX, respectively, may be diverse. We thus intend to optimize these parameters to further reduce current consumptions. Here, we employ the direction cosines of specific unit vector $\boldsymbol{M}$ (see Fig. 6(a)) to computationally adjust them. In particular, we assume that the pulse intensity and width are proportional to direction cosines of RE, TC, and EX, and the direction angles are θ_r for RE, θ_t for TC, and θ_e for EX, satisfying $\cos^2\theta_\text{e} + \cos^2\theta_\text{t} + \cos^2\theta_\text{r} = 1$. Thus, we set $(S_0^\text{r}, S_0^\text{t}, S_0^\text{e}) = S_0(\cos\theta_\text{r}, \cos\theta_\text{t}, \cos\theta_\text{e})$ and $(\delta_0^\text{r}, \delta_0^\text{t}, \delta_0^\text{e}) = \delta_0(|\cos\theta_\text{r}|, |\cos\theta_\text{t}|, |\cos\theta_\text{e}|)$. To exemplify the effectiveness of this method, 3:2 on-off ACC-SARS is taken as an example which corresponds to Figs. 5(d)–5(f). Hence, $\theta_\text{r} \in (0°, 90°)$, $\theta_\text{t} \in (90°, 180°)$, and $\theta_\text{e} \in (90°, 180°)$. During simulation, we randomly select some points, X, Y, Z, on the surface of unit sphere (i.e., $X^2 + Y^2 + Z^2 = 1$, where $X = \cos\theta_\text{r} > 0, Y = \cos\theta_\text{t} < 0$, and $Z = \cos\theta_\text{e} < 0$, see Fig. 6(b)) to represent the ends of stimulation vector $\boldsymbol{M}$ with the origin at (0, 0, 0). Interestingly, Fig. 6(c) shows that in some specific directions (e.g., Θ_1, Θ_2, and Θ_3), SWD can also be thoroughly

abated and, above all, the currents consumed are only one-third of that with no DS. As it is reported that single DBS electrode with multiple contacts[32–33] can perform the DS stimulations by activating several specific contacts, the above stimulation protocol can be approximately compared with DS stimulations, i.e., 3∶2 on-off ACC-DS-SARS. In clinic, it can be performed by 3 contacts of an electrode, due to the fact that RE, TC, and EX are 3 adjacent nuclei in CT network.

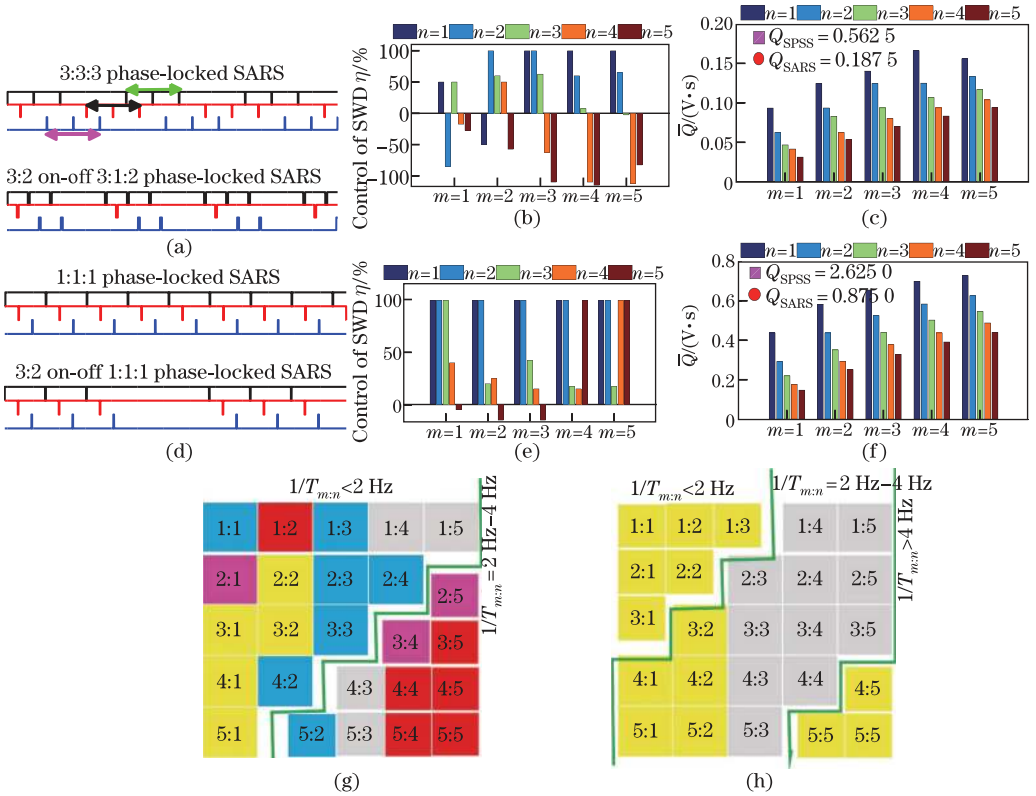

Fig. 5 (a) (3∶2 on-off) ACC-quasi-SARS paradigm simulated by setting $f^0 = 50$ Hz, $\delta_0 = 1$ ms, $|S_0| = 150$ mV, and $T_1 = 36$ ms in Eqs. (8) and (9); (d) (3∶2 on-off) ACC-SARS paradigm simulated by setting $f^0 = 50$ Hz, $\delta_0 = 3.5$ ms, $|S_0| = 200$ mV, and $T_1 = 60$ ms in Eqs. (8) and (9); (b) and (e) the SWD control η, and (c) and (f) the corresponding average current consumption $\overline{Q}$, with respect to the panel of Fig. 3(a), induced by the $m∶n$ on-off ACC-quasi-SARS and ACC-SARS paradigms, respectively. $\overline{Q}$ is calculated by the total charge divided by parameter gird points, where colored "□" and "◯" indicate the current consumptions corresponding to SPSS and SARS, respectively; (g) and (h) the other forms of visualizations corresponding to (b) and (e), respectively, where yellow and blue show that the stimulus can completely abate SWD onsets or reduce the SWD by half, red and purple indicate that stimulus can doubly promote or increase SWD by half, gray means that stimulus just slightly affects SWD, and green lines distinguish the different frequency regions of $m∶n$ on-off stimulations, i.e., $f_{m:n} = (1/T_{m:n})$ <2 Hz, 2 Hz–4 Hz, and >4 Hz (color online)

3.3 Dynamical interpretations for SWD control by SARS

Finally, we dynamically interpret the stimulus-induced SWD abatement. To this end, we calculate the AMFRs and TAMFRs for the neural masses of CT. TAMFRs are determined by AMFRs occurring at the boundary of typical state region. In Fig. 7(a), corresponding to the state transition of Fig. 3(a), by fixing $\nu_{ee} = 0.75$ mV·s, we plot the AMFRs of different state activities for RE, TC, and EX as a function of $-\nu_{tr}$ to observe the activity levels of CT network.

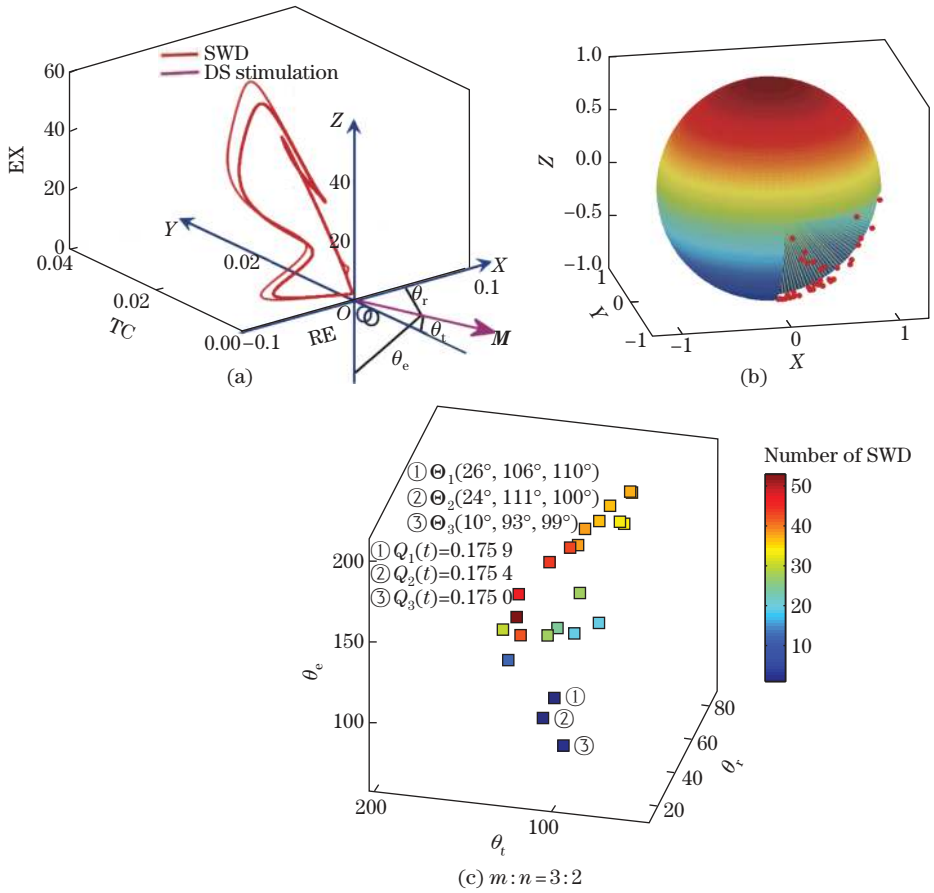

Fig. 6 (a) SWD attractor in the phase portrait spanned by RE, TC, and EX, where the purple arrow $\boldsymbol{M}$ denotes the DS stimulation vector in the coordinate system, $OXYZ$, originated at (0,0,0), and $\theta_{\rm r}, \theta_{\rm t}, \theta_{\rm e}$ are direction angles; (b) randomly selected points satisfying $\theta_{\rm e} \in (90°, 180°)$, $\theta_{\rm t} \in (90°, 180°)$, and $\theta_{\rm r} \in (0°, 90°)$ in the unit sphere; (c) SWD abatement and current consumptions induced by 3∶2 on-off ACC-DS-SARS. It is obtained by fine-tuning the pulse intensity S_0^X and duration δ_0^X of anodic and cathodic pulses of 3∶2 on-off ACC-SARS in the lower panel of Fig. 5(d) (color online)

We find that these AMFRs decrease monotonically as $-\nu_{\rm tr}$ grows. Thus, low-/high-TAMFRs (dashed lines) corresponding to 2 Hz–4 Hz SWD generation/termination exist. Therefore, whether 2 Hz–4 Hz SWD can be abated is dependent on the size relationship between the AMFRs of system and the TAMFRs of 2 Hz–4 Hz SWD. In Figs. 7(b)–7(d), we plot the low and high TAMFRs (the dashed lines fitted by red and blue squares) for RE, TC, and EX, respectively, by scanning $\nu_{\rm ee} \in [0.5\,{\rm mV{\cdot}s},\ 1\,{\rm mV{\cdot}s}]$. This particularly outlines the AMFRs regions corresponding to the stable 2 Hz–4 Hz SWD. When the AMFRs of neurons fall into the region bounded by low-/high-TAMFRs, the system displays the stable 2 Hz–4 Hz SWD. Consistent with Fig. 3(a), the yellow solid circles (as a control, fixing $\nu_{\rm tr} = -0.6\,{\rm mV{\cdot}s}$) fall into the 2 Hz–4 Hz regions, then, the system shows the SWD.

Furthermore, the SWD can also be abated by bidirectionally driving, e.g., increasing or decreasing the AMFRs of RE, TC, and EX that make the system escape from the regions of 2 Hz–4 Hz SWD. Figures 7(b)–7(d) also plot the AMFRs of RE, TC, and EX under various aforementioned stimulus paradigms including ACC-SPSS, ACC-SARS, 3∶2 on-off ACC-(DS-) SARS. The stimulation parameters are the same as Figs. 5 and 6. It is clearly seen that, under the comprehensive functions of the interactions within TC circuit and these specific stimulus

protocols, the AMFRs of EX can be successfully decreased and kicked out of the 2 Hz–4 Hz SWD regions. Thus, the SWD is abated. Reversely, we try to apply the CAA-SARS (black stars) to the system, which is surprisingly shown to largely enhance the AMFR of the system and make it rise far above the 2 Hz–4 Hz SWD region. The system eventually shows the saturated states, resulting in the terminations of the SWD.

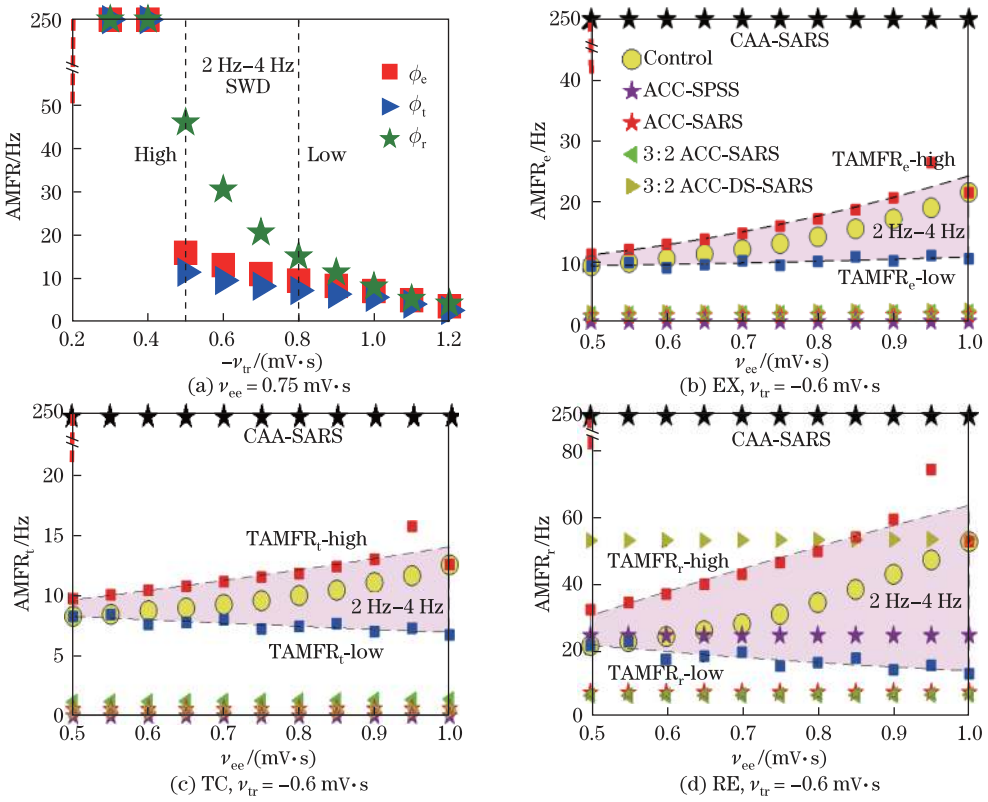

Fig. 7 (a) AMFRs of EX (colored "□"), TC (colored "▷"), and RE (colored "⋆") as a function of $-\nu_{tr}$ with $\nu_{ee} = 0.75$ mV·s, where two dashed lines "high" and "low" represent the occurring positions of 2 Hz–4 Hz SWD; (b), (c), and (d) the AMFRs of EX (b), TC (c), and RE (d) as a function of ν_{ee} with $\nu_{tr} = -0.6$ mV·s, where two gray dashed curves fitted by the blue and red squares denote the two low and high TAMFRs, colored "○", "⋆", "◁", "▷" represent the AMFRs in the absence or presence of various stimulation patterns with ACC pulses of RE, TC, and EX, and black "⋆" indicates the SARS with CAA pulses applied on RE, TC, and EX (color online)

4 Conclusions

In sum, we have computationally proposed a kind of tri-target $m:n$ on-off ACC-SARS stimulation paradigms in terms of suppressing absence seizures. Results suggest that regularized rather than randomly patterned ACC-SARS is more effective to abate the SWD. With respect to saving stimulation current, the $m:n$ on-off ACC-SARS is also superior to ACC-SPSS, which can be further improved by considering the DS stimulation therapy. In addition, the period of $m:n$ on-off ACC-SARS outside the 2 Hz–4 Hz dominant rhythm is suggested to be the better choice in controlling the SWD. At last, AMFRs and TAMFRs demonstrate the effect of these stimulation protocols. Detailed investigations reveal that the SWD can be suppressed by employing SARS

to drive the AMFR of neurons to be out of the regions bounded by the TAMFR of the 2 Hz–4 Hz SWD.

In fact, the stimulation effects vary when stimulus is applied on different targets within CT circuit. In addition, clinical or experimental evidences have demonstrated that both the low[34–35] and high[14,36] frequency stimulations can be effective in suppressing the seizures. In particular, it is reported that the seizures can be decreased by the stimulations of cortex with low-frequency pulses[35]. Given energy saving and less tissue damage, here our primary concern is on the effects of low frequency stimulations for the seizure abatement. Results show that the effective stimulation frequency can be further reduced by using the newly proposed $m:n$ on-off SARS protocol, which is particularly close to the 2 Hz–4 Hz dominant frequency wave rhythm of the SWD.

Note that, the proposed SARS protocol is actually the special case of the classic coordinated reset (CR) stimulation[37–43]. In our future work, we will particularly focus on the effect of the demand-based CR stimulation[44] that involves in the specific stimulation timing and length. In addition, the CR stimulation usually considers charge-balanced pulses[45–47]. More generally, in future we will also concern the effect of the specific forms of pulse stimulation[48] on absence seizures.

References

[1] AGHAKHANI, Y., BAGSHAW, A. P., BENAR, C. G., HAWCO, C., ANDERMANN, F., DUBEAU, F., and GOTMAN, J. fMRI activation during spike and wave discharges in idiopathic generalized epilepsy. *Brain*, **127**(5), 1127–1144 (2004)

[2] PINAULT, D. and O'BRIEN, T. J. Cellular and network mechanisms of genetically-determined absence seizures. *Thalamus Related Systems*, **3**(3), 181–203 (2005)

[3] TENNEY, J. R., DUONG, T. Q., KING, J. A., LUDWIG, R., and FERRIS, C. F. Corticothalamic modulation during absence seizures in rats: a functional MRI assessment. *Epilepsia*, **44**(9), 1133–1140 (2003)

[4] MIAO, A., WANG, Y., XIANG, J., LIU, Q., CHEN, Q., QIU, W., LIU, H., TANG, L., GAO, Y., WU, C., YU, Y., SUN, J., JIANG, W., SHI, Q., ZHANG, T., HU, Z., and WANG, X. Ictal source locations and cortico-thalamic connectivity in childhood absence epilepsy: associations with treatment response. *Brain Topography*, **32**(1), 178–191 (2019)

[5] YANG, D. P. and ROBINSON, P. A. Unified analysis of global and focal aspects of absence epilepsy via neural field theory of the corticothalamic system. *Physical Review E*, **100**(3), 032405 (2019)

[6] WANG, R. B., ZHANG, Z. K., and CHI, K. T. Neurodynamics analysis of brain information transmission. *Applied Mathematics and Mechanics* (*English Edition*), **30**(11), 1415–1428 (2009) https://doi.org/10.1007/s10483-009-1107-y

[7] KOLASSA, I. T., WIENBRUCH, C., NEUNER, F., SCHAUER, M., RUF, M., ODENWALD, M., and ELBERT, T. Altered oscillatory brain dynamics after repeated traumatic stress. *BMC Psychiatry*, **7**(1), 56 (2007)

[8] GUO, J., BISWAL, B. B., HAN, S., LI, J., YANG, S., YANG, M., and CHEN, H. Altered dynamics of brain segregation and integration in poststroke aphasia. *Human Brain Mapping*, **40**(11), 3398–3409 (2019)

[9] GRANNAN, E. R., KLEINFELD, D., and SOMPOLINSKY, H. Stimulus-dependent synchronization of neuronal assemblies. *Neural Computation*, **5**(4), 550–569 (1993)

[10] LEWIS, C. M., BOSMAN, C. A., WOMELSDORF, T., and FRIES, P. Stimulus-induced visual cortical networks are recapitulated by spontaneous local and interareal synchronization. *Proceedings of the National Academy of Sciences*, **113**(5), E606–E615 (2016)

[11] LIANG, S. and WANG, Z. Controlling a neuron by stimulating a coupled neuron. *Applied Mathematics and Mechanics* (*English Edition*), **40**(1), 13–24 (2019) https://doi.org/10.1007/s10483-019-2407-8

[12] SALANOVA, V. Deep brain stimulation for epilepsy. *Epilepsy and Behavior*, **88**, 21–24 (2018)

[13] LODDENKEMPER, T., PAN, A., NEME, S., BAKER, K. B., REZAI, A. R., DINNER, D. S., MONTGOMERY, E., JR, and LÜDERS, H. O. Deep brain stimulation in epilepsy. *Journal of Clinical Neurophysiology*, **18**(6), 514–532 (2001)

[14] OSORIO, I., OVERMAN, J., GIFTAKIS, J., and WILKINSON, S. B. High frequency thalamic stimulation for inoperable mesial temporal epilepsy. *Epilepsia*, **48**(8), 1561–1571 (2007)

[15] WANG, Z. and WANG, Q. Eliminating absence seizures through the deep brain stimulation to thalamus reticular nucleus. *Frontiers in Computational Neuroscience*, **11**, 22 (2017)

[16] YAMAMOTO, J., IKEDA, A., SATOW, T., TAKESHITA, K., TAKAYAMA, M., MATSUHASHI, M., MATSUMOTO, R., OHARA, S., MIKUNI, N., TAKAHASHI, T., MIYAMOTO, S., TAKI, W., HASHIMOTO, N., ROTHWELL, J. C., and SHIBASAKI, H. Low-frequency electric cortical stimulation has an inhibitory effect on epileptic focus in mesial temporal lobe epilepsy. *Epilepsia*, **43**(5), 491–495 (2002)

[17] CHEN, M., GUO, D., WANG, T., JING, W., XIA, Y., XU, P., LUO, C., VALDES-SOSA, P. A., and YAO, D. Z. Bidirectional control of absence seizures by the basal ganglia: a computational evidence. *PLoS Computational Biology*, **10**(3), e1003495 (2014)

[18] CHEN, M., GUO, D., LI, M., MA, T., WU, S., MA, J., CUI, Y., XIA, Y., XU, P., and YAO, D. Z. Critical roles of the direct GABAergic pallido-cortical pathway in controlling absence seizures. *PLoS Computational Biology*, **11**(10), e1004539 (2015)

[19] HOLMES, M. D., BROWN, M., and TUCKER, D. M. Are generalized seizures truly generalized? Evidence of localized mesial frontal and frontopolar discharges in absence. *Epilepsia*, **45**(12), 1568–1579 (2004)

[20] ROBINSON, P. A., RENNIE, C. J., WRIGHT, J. J., and BOURKE, P. D. Steady states and global dynamics of electrical activity in the cerebral cortex. *Physical Review E*, **58**(3), 3557–3571 (1998)

[21] WRIGHT, J. J. and LILEY, D. T. J. Dynamics of the brain at global and microscopic scales: neural networks and the EEG. *Behavioral and Brain Sciences*, **19**(2), 285–295 (1996)

[22] ROBINSON, P. A., RENNIE, C. J., and ROWE, D. L. Dynamics of large-scale brain activity in normal arousal states and epileptic seizures. *Physical Review E*, **65**(4), 041924 (2002)

[23] RUBIN, J. E. and TERMAN, D. High frequency stimulation of the subthalamic nucleus eliminates pathological thalamic rhythmicity in a computational model. *Journal of Computational Neuroscience*, **16**(3), 211–235 (2004)

[24] GUO, Y., RUBIN, J. E., MCINTYRE, C. C., VITEK, J. L., and TERMAN, D. Thalamocortical relay fidelity varies across subthalamic nucleus deep brain stimulation protocols in a data-driven computational model. *Journal of Neurophysiology*, **99**(3), 1477–1492 (2008)

[25] FAN, D. and WANG, Q. Closed-loop control of absence seizures inspired by feedback modulation of basal ganglia to the corticothalamic circuit. *IEEE Transactions on Neural Systems and Rehabilitation Engineering*, **28**(3), 581–590 (2020)

[26] FAN, D. and WANG, Q. Improved control effect of absence seizures by autaptic connections to the subthalamic nucleus. *Physical Review E*, **98**(5), 052414 (2018)

[27] ERMENTROUT, B. Simulating, analyzing, and animating dynamical systems: a guide to XPPAUT for researchers and students. *Applied Mechanics Reviews*, **56**(4), B53 (2003)

[28] FAN, D., WANG, Q., SU, J., and XI, H. Stimulus-induced transitions between spike-wave discharges and spindles with the modulation of thalamic reticular nucleus. *Journal of Computational Neuroscience*, **43**(3), 203–225 (2017)

[29] GE, Y., CAO, Y., YI, G., HAN, C., QIN, Y., WANG, J., and CHE, Y. Robust closed-loop control of spike-and-wave discharges in a thalamocortical computational model of absence epilepsy. *Scientific Reports*, **9**(1), 1–16 (2019)

[30] YIN, L., ZHENG, R., KE, W., HE, Q., ZHANG, Y., LI, J., WANG, B., MI, Z., LONG, Y. S., and RASCH, M. J. Autapses enhance bursting and coincidence detection in neocortical pyramidal cells. *Nature Communications*, **9**(1), 1–12 (2018)

[31] KE, W., HE, Q., and SHU, Y. Functional self-excitatory autapses (auto-synapses) on neocortical pyramidal cells. *Neuroscience Bulletin*, **35**(6), 1106–1109 (2019)

[32] CONTARINO, M. F., BOUR, L. J., VERHAGEN, R., LOURENS, M. A., DE BIE, R. M., VAN DEN MUNCKHOF, P., and SCHUURMAN, P. R. Directional steering: a novel approach to deep brain stimulation. *Neurology*, **83**(13), 1163–1169 (2014)

[33] MARTENS, H. C. F., TOADER, E., DECRE, M. M. J., ANDERSON, D. J., VETTER, R., KIPKE, D. R., BAKER, K. B., JOHNSON, M. D., and VITEK, J. L. Spatial steering of deep brain stimulation volumes using a novel lead design. *Clinical Neurophysiology*, **122**(3), 558–566 (2011)

[34] KILE, K. B., TIAN, N., and DURAND, D. M. Low frequency stimulation decreases seizure activity in a mutation model of epilepsy. *Epilepsia*, **51**(9), 1745–1753 (2010)

[35] YAMAMOTO, J., IKEDA, A., KINOSHITA, M., MATSUMOTO, R., SATOW, T., TAKESHITA, K., MATSUHASHI, M., MIKUNI, N., MIYAMOTO, S., HASHIMOTO, N., and SHIBASAKI, H. Low-frequency electric cortical stimulation decreases interictal and ictal activity in human epilepsy. *Seizure*, **15**(7), 520–527 (2006)

[36] NELSON, T. S., SUHR, C. L., FREESTONE, D. R., LAI, A., HALLIDAY, A. J., MCLEAN, K. J., BURKITT, A. N., and COOK, M. J. Closed-loop seizure control with very high frequency electrical stimulation at seizure onset in the gaers model of absence epilepsy. *International Journal of Neural Systems*, **21**(2), 163–173 (2011)

[37] TASS, P. A., SILCHENKO, A. N., HAUPTMANN, C., BARNIKOL, U. B., and SPECKMANN, E. J. Long-lasting desynchronization in rat hippocampal slice induced by coordinated reset stimulation. *Physical Review E*, **80**(1), 011902 (2009)

[38] LYSYANSKY, B., POPOVYCH, O. V., and TASS, P. A. Desynchronizing anti-resonance effect of m:n on-off coordinated reset stimulation. *Journal of Neural Engineering*, **8**(3), 036019 (2011)

[39] KUBOTA, S. and RUBIN, J. E. Numerical optimization of coordinated reset stimulation for desynchronizing neuronal network dynamics. *Journal of Computational Neuroscience*, **45**(1), 45–58 (2018)

[40] ADAMCHIC, I., TOTH, T., HAUPTMANN, C., WALGER, M., LANGGUTH, B., KLINGMANN, I., and TASS, P. A. Acute effects and after-effects of acoustic coordinated reset neuromodulation in patients with chronic subjective tinnitus. *NeuroImage*: *Clinical*, **15**, 541–558 (2017)

[41] GUO, Y. and RUBIN, J. E. Multi-site stimulation of subthalamic nucleus diminishes thalamocortical relay errors in a biophysical network model. *Neural Networks*, **24**(6), 602–616 (2011)

[42] TASS, P. A. and HAUPTMANN, C. Anti-kindling achieved by stimulation targeting slow synaptic dynamics. *Restorative Neurology and Neuroscience*, **27**(6), 591–611 (2009)

[43] TASS, P. A., QIN, L., HAUPTMANN, C., DOVERO, S., BEZARD, E., BORAUD, T., and MEISSNER, W. G. Coordinated reset has sustained aftereffects in Parkinsonian monkeys. *Annals of Neurology*, **72**(5), 816–820 (2012)

[44] TASS, P. A. A model of desynchronizing deep brain stimulation with a demand-controlled coordinated reset of neural subpopulations. *Biological Oybernetics*, **89**(2), 81–88 (2003)

[45] LILLY, J. C., HUGHES, J. R., ALVORD, E. C., JR, and GALKIN, T. W. Brief, noninjurious electric waveform for stimulation of the brain. *Science*, **121**, 468–469 (1955)

[46] MORTIMER, J. T., SHEALY, C. N., and WHEELER, C. Experimental nondestructive electrical stimulation of the brain and spinal cord. *Journal of Neurosurgery*, **32**(5), 553–559 (1970)

[47] HARNACK, D., WINTER, C., MEISSNER, W., REUM, T., KUPSCH, A., and MORGENSTERN, R. The effects of electrode material, charge density and stimulation duration on the safety of high-frequency stimulation of the subthalamic nucleus in rats. *Journal of Neuroscience Methods*, **138**, 207–216 (2004)

[48] GRILL, W. M. Model-based analysis and design of waveforms for efficient neural stimulation. *Progress in Brain Research*, **222**, 147–162 (2015)